Hydrographic and Biological Survey of a Surface-Intensified Anticyclonic Eddy in the Caribbean Sea

van der Boog, C. G.; de Jong, M. F.; Scheidat, M.; Leopold, M. F.; Geelhoed, S. C.V.; Schulz, K.; Pietrzak, J. D.; Katsman, C. A.; Dijkstra, H.A.

DOI
10.1029/2018JC014877

Publication date
2019

Document Version
Final published version

Published in
Journal of Geophysical Research: Oceans

JGR Oceans

RESEARCH ARTICLE
10.1029/2018JC014877

Hydrographic and Biological Survey of a Surface-Intensified Anticyclonic Eddy in the Caribbean Sea

C. G. van der Boog[1], M. F. de Jong[2], M. Scheidat[3], M. F. Leopold[3], S. C. V. Geelhoed[3], K. Schulz[4,5], H. A. Dijkstra[6], J. D. Pietrzak[1], and C. A. Katsman[1]

[1]Environmental Fluid Mechanics, Civil Engineering and Geosciences, Delft University of Technology, Delft, The Netherlands, [2]Royal Netherlands Institute for Sea Research, Den Burg, The Netherlands, [3]Wageningen Marine Research, Den Helder, The Netherlands, [4]Royal Netherlands Institute for Sea Research, Yerseke, The Netherlands, [5]Now at AWI, Bremen, Germany, [6]Institute for Marine and Atmospheric Research, Utrecht University, Utrecht, The Netherlands

Key Points:
- Observed velocities (0.72 m/s) of the 180-km-wide eddy are strongly surface intensified
- At the front, higher densities of flying fish but no species at higher trophic levels were observed
- The eddy core contained river water and a strong subsurface temperature inversion (0.98°C)

Correspondence to:
C. G. van der Boog,
c.g.vanderboog@tudelft.nl

Citation:
van der Boog, C. G., de Jong, M. F., Scheidat, M., Leopold, M. F., Geelhoed, S. C. V., Schulz, K., et al. (2019). Hydrographic and biological survey of a surface-intensified anticyclonic eddy in the Caribbean Sea. *Journal of Geophysical Research: Oceans*, *124*. https://doi.org/10.1029/2018JC014877

Received 17 DEC 2018
Accepted 15 JUL 2019
Accepted article online 30 JUL 2019

Abstract In the Caribbean Sea, mesoscale anticyclonic ocean eddies impact the local ecosystem by mixing of low salinity river outflow with the nutrient-rich waters upwelling along the Venezuelan and Colombian coast. To gain insight into the physics and the ecological impact of these anticyclones, we performed a combined hydrographic and biological survey of one Caribbean anticyclone in February 2018. We found that the anticyclone had a radius of 90 km and was surface intensified with the strongest velocities (0.72 m/s) in the upper 150 m of the water column. Below, isopycnal displacements were found down to 700 dbar. The core of the anticyclone entrained waters from the Orinoco River plume and contained slightly elevated chlorophyll concentrations compared to the surroundings. At the edge of the anticyclone we observed higher densities of flying fish but not higher densities of predators like seabirds and cetaceans. Below the surface, a strong temperature inversion (0.98 °C) was present within a barrier layer. In addition, we found thermohaline staircases that originated from double diffusion processes within Tropical Atlantic Central Water.

1. Introduction

In the Caribbean Sea, two major nutrient sources are available: the wind-driven upwelling along the Venezuelan and Colombian coast and the plumes of the Amazon and Orinoco River that are advected into the basin (Bidigare et al., 1993; Gilbes & Armstrong, 2004; Molleri et al., 2010; Morell & Corredor, 2001; Rueda-Roa & Muller-Karger, 2013). These two nutrient sources are mixed with the oligotrophic surrounding waters by mesoscale eddy activity (Alvera-Azcárate et al., 2009; Corredor et al., 2004; Hu et al., 2004). The eddies in the Caribbean Sea are predominantly anticyclonic and have diameters ranging from 50–200 km (Andrade & Barton, 2000; Gaube et al., 2015). They are generated in the eastern part of the basin, where the river plumes form strong fronts (Corredor et al., 2003). The anticyclones intensify on their path westward while passing the upwelling region. There, the anticyclones advect cold filaments of nutrient-rich upwelled waters northward. Ocean circulation models have been used to show that this advection results in the offshore cooling of Caribbean surface waters (Jouanno & Sheinbaum, 2013).

The anticyclones alter the ecosystem by the advection and dispersal of biota (Ezer et al., 2005) and by the advection of patches containing water from the river plumes (Corredor et al., 2004). Based on ocean color images, Chérubin and Richardson (2007) showed that after the river plume arrives the eddy kinetic energy increases, and they concluded that this enhancement results in considerable flow variability in the Caribbean coastal ecosystems. At greater depths, the flow is less variable and susceptible to the formation of thermohaline staircases, which form from double diffusive processes (Merryfield, 2000). Morell et al. (2006) suggest that Caribbean eddies, both cyclones and anticyclones, could alter these staircase structures. Farther downstream, anticyclones influence the frequency of the shedding of large Loop Current Rings (Oey et al., 2003), a pronounced oceanic feature in the Gulf of Mexico (Oey et al., 2005).

Despite this impact of the Caribbean anticyclones on the local ecosystem, the physical processes governing the origin and development of the anticyclones remain unclear. Some modeling studies suggest that

wind is the dominant driver (Chang & Oey, 2013; Oey et al., 2003), while others argue, based on idealized models and surface drifters, that Caribbean anticyclones are formed of remnants of North Brazil Current (NBC) Rings (Richardson, 2005; Simmons & Nof, 2002). Furthermore, modeling studies show that mixed barotropic-baroclinic instabilities of the Caribbean Current can generate and intensify the anticyclones (Jouanno et al., 2008, 2009).

Additional observations are necessary to clarify the origin and physics of the development of the Caribbean anticyclones. Until now, observations were based on surface drifter data (Centurioni & Niiler, 2003; Molinari et al., 1981; Richardson, 2005) and satellite altimetry (e.g., Alvera-Azcárate et al., 2009; Nystuen & Andrade, 1993). Although these studies provide valuable information about the size and surface properties of the anticyclones, they do not provide details on their vertical structure. These can be obtained from dedicated surveys of eddies in the Caribbean Sea (Corredor et al., 2004; Morell et al., 2006; Rudzin et al., 2017; Silander, 2005). Rudzin et al. (2017) performed upper ocean observations of a Caribbean anticyclone and showed that the anticyclone contained a barrier layer, which is the layer between a shallow halocline and deeper thermocline. Barrier layers store heat below the mixed layer and affect the local weather when this heat is released (Rudzin et al., 2017). In the other surveys (Corredor et al., 2004; Morell et al., 2006; Silander, 2005), the emphasis is on the biogeochemical properties of cyclones. Although the eddies in the Caribbean Sea are predominantly anticyclonic, their biogeochemical properties have not been studied before.

To study the origin, vertical structure, and ecological impact of Caribbean anticyclones, we performed a combined biological and hydrographic survey of a Caribbean anticyclone in February 2018. With these observations, we can deduce the origin of this anticyclone and its impact on the local ecosystem. We provide details on the survey in section 2 and describe the evolution and vertical structure of the targeted anticyclone in section 3. Afterward, the upper ocean characteristics (mixed layer, the barrier layer, and the thermohaline staircases) of the observations are discussed. The effects of hydrodynamic features on biological processes are investigated in section 4. The results are summarized and discussed in section 5. An overview of the hydrographic properties, including a water mass analysis, is given in the Appendix.

2. Materials and Methods

2.1. In Situ Measurements

Figure 1 shows the track of the survey performed between 4 and 11 February 2018 on the RV *Pelagia*, which started in Aruba and ended in St. Maarten. The hydrographic data consist of 15 CTD (conductivity, temperature, depth) stations that were located between the islands of Aruba and Hispaniola and underway data from an aquaflow system. In addition, upper ocean current velocities were obtained with a vessel-mounted acoustic Doppler current profiler (VMADCP). Visual surveys of birds and pelagic megafauna were conducted during daylight hours along the cruise track. The locations of survey stations were chosen based on the altimetric signature of an anticyclone in the weeks leading up to the cruise. Based on these analyses, the center of this 180-km-wide anticyclone was expected north of Aruba at the start of the cruise. Four Argo floats were deployed during the survey to gain insight on the evolution of the temperature and salinity of Caribbean waters.

The 75-kHz VMADCP mounted under the RV *Pelagia* collected flow velocity data along the transect. While drifting at stations, the VMADCP was turned off to limit interference with acoustic monitoring of the pelagic fauna. For the results of the acoustic monitoring we refer to de Jong (2018). The VMADCP provided horizontal current velocities below the vessel down to approximately 600-m depth with a vertical resolution of 16 m. The blanking distance below the vessel was 25 m. The temporal resolution of the ensembles is 10 min, and each ensemble was averaged over 150 pings. Tidal velocities were estimated with the TPXO9 model (Egbert & Erofeeva, 2002) and removed from the VMADCP data with Cascade V7.2 (Kermabon et al., 2018). Furthermore, a quality check of the VMADCP data was performed by using Cascade V7.2 (Kermabon et al., 2018).

Stations were planned on a line across the anticyclone and continued to the north outside the eddy to observe the background hydrography of the Caribbean Sea (Figure 1). The distance between the stations across the eddy is 38.9 km, which is less than half the radius of the eddy (R = 90 km). North of the eddy the stations are separated farther apart with a station distance of 61.4 km over the deep basin. The station distance was smaller (30 km) over the continental slope close to Hispaniola. Stations 1, 2, 3, 8, 12, 13, 14, and 15 were

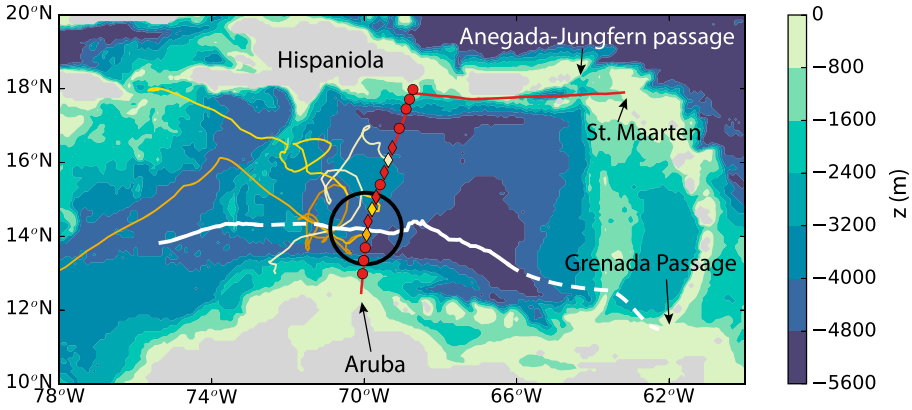

Figure 1. Bathymetry (m) of the eastern Caribbean Sea showing the cruise track (red line) and track of the center of the eddy (white line). The black circle indicates the location of the anticyclone, estimated from satellite altimetry, at the time of the survey. The track is obtained with the py-eddy tracker of Mason et al. (2014; white solid line) and extended with visual tracking of sea level anomalies (white dashed line). Hydrographic stations along the cruise track that were sampled down to the bottom and down to 2,000 m are shown with dots and diamonds, respectively. Red markers indicate hydrographic stations and yellow markers indicate hydrographic stations where Argo floats were also deployed. The tracks of the Argo floats from February 2018 to September 2018 are shown with the yellow solid lines.

sampled down to the bottom. Stations 4, 5, 6, 7, 9, 10, and 11 were sampled down to 2,000 m to save time needed for horizontal resolution.

At each station, vertical profiles of temperature, salinity, oxygen, chlorophyll, and turbidity were obtained with a CTD system. Physical parameters and oxygen were measured with a SeaBird Electronics 911 system, Wetlabs and Chelsea Aqua sensors provided measurements of turbidity and chlorophyll (for further details see de Jong, 2018). At each station, water samples were taken for salinity calibration. The calibrated CTD data were averaged to vertical bins of 1 dbar. In addition, nutrients samples for phosphate, silicate, nitrate, and nitrite were collected from all 15 stations with the CTD-rosette with a vertical spacing of 25 dbar in the upper 100 dbar. The vertical spacing increased to 50 dbar down to 250 dbar. Below 250 dbar, nutrient samples were taken every 250 dbar. At each station, the sample depth closest to the chlorophyll maximum was adjusted slightly to specifically sample the chlorophyll maximum. The depth of this maximum was determined from the downcast of the CTD. Unfortunately, it was not possible during this cruise to perform water sample analysis of oxygen and chlorophyll. We therefore focus on relative differences within and between profiles, rather than absolute values. Two Argo floats were deployed at Station 4, and single Argo floats were deployed at Stations 6 and 10 (yellow diamonds in Figure 1). These Argo floats sampled temperature and conductivity every 3 days from the surface down to 2,000 dbar to gain insight on the variability of these properties within the Caribbean Sea. During these 3 days, the floats had a parking depth of 500 dbar to avoid grounding on shallow topography downstream.

Surveys of pelagic megafauna took place during daylight hours whenever RV *Pelagia* was sailing. The observation platform is located on top of the bridge, at 9 m above sea level. Seabirds, marine mammals, and flying fish (when visible) were recorded by a team of two to four observers, within a 300-m-wide strip on the side of the vessel that offered the best viewing conditions. In addition to these strip counts, all animals seen within a 180° scan ahead (port to starboard) were recorded (Tasker et al., 1984). All animals seen were logged per 10-min counts. The behavior of observed birds and marine mammals was noted according to the standardized coding method described in Camphuysen and Garthe (2004). In addition, the central position and time, as well as environmental conditions, were recorded for each 10-min count.

2.2. Complementary Data

Prior to, during, and following the survey, the evolution of the anticyclone was studied with gridded sea level anomaly (SLA) fields from satellite altimetry. These fields with a resolution of 0.25° were downloaded from the Copernicus Marine Environment Monitoring Service (CMEMS; http://marine.copernicus.eu). The track of the anticyclone was obtained from the gridded SLA fields with the py-eddy tracker of Mason et al. (2014) that identified circular SLAs as eddies. Negative anomalies were identified as cyclones, positive anomalies as anticyclones. If a SLA signal was not sufficiently circular in shape, it was not considered an eddy. To detect

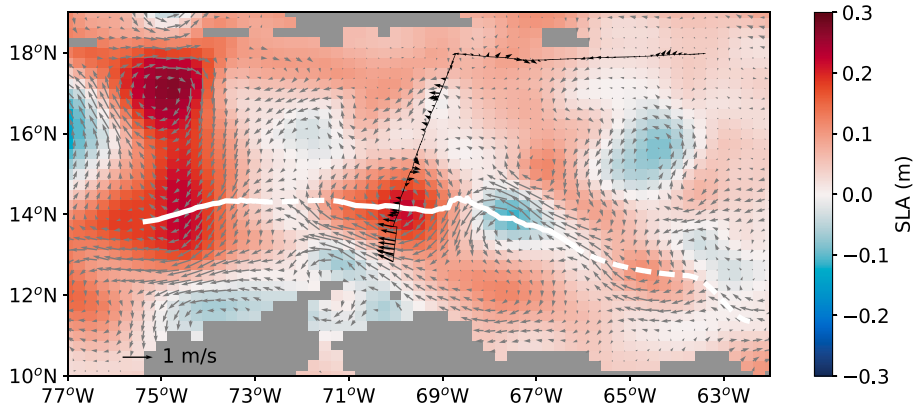

Figure 2. Gridded sea level anomaly (m) on 5 February 2018 with the geostrophic surface velocities (gray vectors) obtained from gridded altimetry from E.U. Copernicus Marine Service Information. The cruise track is indicated by the solid black line. The black arrows show the velocities of the acoustic Doppler current profiler, averaged over the upper 25–35 m (below the blanking distance). The white line indicates the track of the anticyclone.

the origin of the disturbance, the track obtained with the py-eddy tracker was extended by visual analysis of the altimetry product.

In addition to the gridded SLA fields, we applied the py-eddy tracker to daily fields of the global forecast available from CMEMS. The forecasting model, referred to as Mercator, is based on NEMO (Madec, 2015). In this model, the SLA fields of the satellite altimetry and in situ temperature and salinity profiles of the Argo floats are assimilated. The model has a spatial resolution of 1/12°.

Globcolour images were used to analyze the spatial distribution of surface chlorophyll (Bertrand et al., 2009). These gridded images are a merged product from multiple satellite missions and have a spatial resolution of 4.63 km (4.63×4.63 km^2) and temporal resolution of 1 day. The images were generated using CMEMS products at the production center ACRI-ST. The salinity anomaly of the surveyed anticyclone was analyzed with the along-track salinity observations from the Level 2 Ocean Salinity Output from the Soil Moisture and Ocean Salinity satellite obtained from the European Space Agency (http://earth.esa.int).

3. Upper Ocean Characteristics

3.1. Eddy Characteristics

The targeted anticyclone was first detected by the py-eddy tracker as a coherent structure on 28 December 2017. At that time, the Mercator model indicated that the anticyclone had a surface salinity of 34.6 psu and temperature of 28.6 °C. The anticyclone became more saline and colder on its path westward which can be attributed to mixing with the surrounding (colder and more saline) waters and to interaction with the atmosphere. The visual analysis of the altimetry data suggested that the anticyclone originated from a disturbance which could be traced back to Grenada Passage on 11 September 2017 (Figure 1). On average, the anticyclone had a westward propagation velocity of 0.1 m/s, which is on the order of the mean zonal velocity of the Caribbean Current (Richardson, 2005).

At the time of the survey, the center of the anticyclone was located at 14.1°N and 69.8°W. The SLA and geostrophic velocities from altimetry data show that the center of the anticyclone was captured by our observations (Figure 2). The near-surface velocity field obtained from the acoustic Doppler current profiler is similar to that derived from satellite altimetry, and it suggests that the eddy was close to geostrophic balance. This is confirmed by the low Rossby and Burger numbers of the anticyclone (Table 1). The largest surface speed (0.72 m/s) was found 90 km south of the center of the anticyclone, while the flow 90 km north of the anticyclone was weaker (0.41 m/s). This difference in surface velocity was induced by the Caribbean Current, which interacted with the southern part of the anticyclone at that moment. The diameter of the anticyclone was 180 km.

Satellite altimetry indicated that the anticyclone had a SLA of 0.20 m during the survey (Figure 3a). The VMADCP velocities show that the anticyclone was surface intensified, with the strongest velocities

Table 1
Eddy Characteristics on 5 February 2018

Characteristics	Symbols	Magnitude
Sea level anomaly	A	0.20 m
Swirl velocity	U	0.41–0.72 m/s
Depth scale	D	$\mathcal{O}$(150 m)
Radius	R	90 km
Rossby number	$Ro = \frac{U}{f_0 R}$	0.03–0.06
Brunt-Väisälä frequency	$N = \sqrt{-\frac{g}{\rho_0}\frac{\partial \rho}{\partial z}}$	0–0.03 s^{-1}
Burger number	$Bu = \frac{N^2 D^2}{f_0^2 R^2}$	0–0.12

*Note.*The amplitude is obtained from altimetry. The velocity, depth scale, and radius are obtained from the vessel-mounted acoustic Doppler current profiler. The vertical stratification is taken from the CTD measurements. The minimal and maximum Brunt-Väisälä frequency and Burger number are both indicated. Other parameters used to estimate the variables are $f_0 = 1.4 \times 10^{-4}$ s^{-1}, g = 9.81 m/s^2, and $\rho_0 = 1,028$ kg/m^3.

(>0.5 m/s) in the upper 150 m of the eddy (Figure 3b). Below that depth, the swirl velocities were smaller than 0.1 m/s. The weak velocities were induced by small isopycnal displacements, which were found down to 700 dbar. This implies that the anticyclone was baroclinic and had a relatively weak barotropic component. It is plausible that the weak isopycnal displacements were induced by the mass of the anticyclone above, meaning that only the surface waters were advected with the anticyclone. This view is supported by the path of the Argo floats that were deployed in the core of the anticyclone. These Argo floats had a parking depth of 500 dbar and diverted from the path of the anticyclone after deployment (Figure 1).

The surface-intensified velocity structure of the anticyclone is clearly visible in the vertical shear of the anticyclone (Figure 3c). The shear is strongest at the flanks of the anticyclone between 13°N and 15°N below the thermocline (red line in Figure 3c), which indicates that the strongest velocities of the anticyclone are confined to the isothermal layer. In line with Mignot et al. (2012), we defined the depth of the thermocline ($D_{T^*-0.2}$) as the depth where the temperature decreased by 0.2 °C compared to the temperature of the mixed layer. The depth of the halocline ($D_{S^*\pm 0.06}$) was defined as the depth where the salinity deviates from the salinity of the mixed layer (S^*) by $\Delta S_A = 0.06$ g/kg. Interestingly, the strongest shear was not found at the bottom of the mixed layer, but it was found deeper below the thermocline.

The surface of the anticyclone was less saline ($\Delta S_A = -0.2$ g/kg) and warmer ($\Delta T = +0.2$ °C) than the surrounding waters (Figures 3d and 3e). The combined temperature and salinity difference of the anticyclone corresponds to a surface density difference of $\Delta \rho = -0.46$ kg/m^3 between the core of the anticyclone and the surface waters to the north. The maximum temperature of the anticyclone was 28.0 °C and was located at approximately 90 dbar (Figure 3d). This subsurface maximum reflects a temperature inversion and is discussed in section 3.3.

The combination of the salinity anomaly of the anticyclone and the slightly (but significant) elevated silicate levels (Figure A1e) suggested that the anticyclone entrained river outflow. Apparently, the anticyclone originated at Grenada Passage close to the outflow of the Orinoco River in September 2017. At that time, the discharge of the Orinoco River was high (Figure 4a), while the plume of the Amazon River had not yet arrive at this location. This made it plausible that the anticyclone entrained water from the Orinoco River plume and propagated westward with the mean flow. We found in sea surface salinity observations from the "Soil Moisture and Ocean Salinity" satellite that a few days prior to the cruise, on 29 January 2018, the core of the anticyclone contained a low salinity anomaly (Figure 4b), of which a weak signal was still observed at the time of the cruise (Figure 3e). This view is in line with the results of the Mercator model, where the salinity of the anticyclone was relatively low at the start of the track (34.6 psu) and increased on its path westward.

The evolution of the anticyclone after the survey was analyzed with gridded SLA obtained from satellite altimetry and from the output of the Mercator model. This analysis showed that the surveyed anticyclone interacted with a second anticyclone (SLA = +0.29 m) that was located at 16.6°N and 75.4°W during the survey (Figure 2). This first resulted in a small weakening of the SLA signal of the surveyed anticyclone

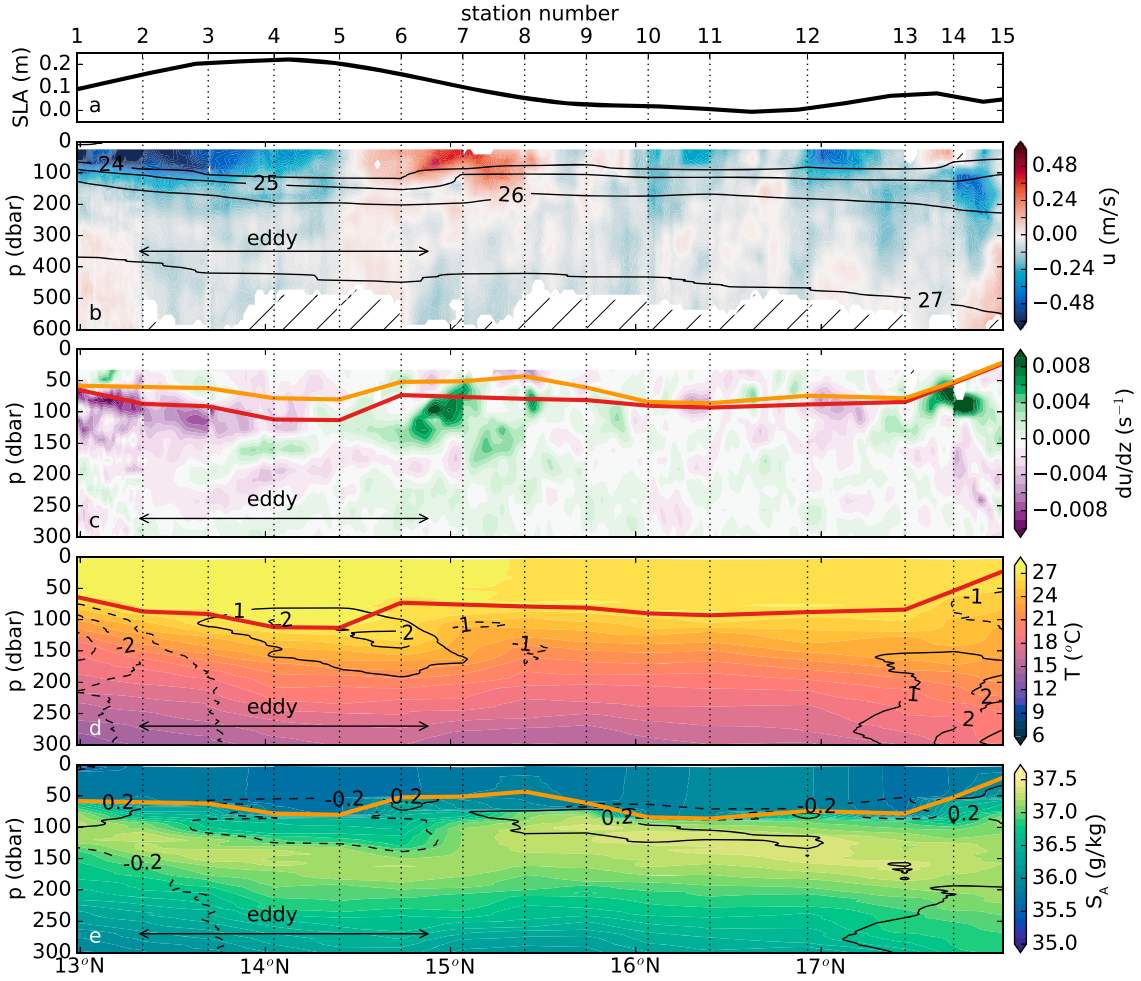

Figure 3. (a) Sea level anomaly (SLA) in m on 5 February 2018 from satellite gridded altimetry obtained from Copernicus Marine Environment Monitoring Service. (b) Zonal velocity (m/s) along the cruise track. Positive velocities are in eastward direction. The hatched regions indicate where vessel-mounted acoustic Doppler current profiler data were rejected due to poor backscatter. The black contour lines show the isopycnals. (c) Vertical shear (s^{-1}) along the cruise track. (d) Conservative temperature (°C) obtained from CTD profiles. The black contour lines show temperature deviations from the mean temperature profile. (e) Absolute salinity (g/kg). The black contour lines show salinity deviations from the mean salinity profile. Both temperature and salinity are interpolated along the survey from the profiles obtained at the stations. The thermocline and halocline, indicated with the red and orange lines, respectively, were computed following Mignot et al. (2012).

(SLA = +0.18 m). On 13 March 2018, the two anticyclones merged into one anticyclone with a maximum SLA of SLA = +0.30 m that propagated farther westward. Previous modeling studies suggested that Caribbean anticyclones get more energetic on their path westward through baroclinic instabilites (Carton & Chao, 1999; Jouanno et al., 2009). However, this merging process illustrates that anticyclones can also get more energetic through merging and indicates that not all anticyclones develop in the same manner.

3.2. Mixed Layer Depth and Chlorophyll

The Caribbean Sea has a seasonal cycle in mixed layer depths driven by the north-south movement of the Intertropical Convergence Zone and the associated intensification of the northeasterly trade winds over the basin during boreal winter (Taylor & Alfaro, 2005). Montoya-Sánchez et al. (2018) determined a climatology of air-sea heat exchange and mixed layer depth using atmosphere and ocean reanalyses. They conclude that surface cooling and mixed layer deepening is predominantly caused by the latent heat loss caused by the trade winds. Winter mixed layer depths are typically around 50-m depth, with slightly shallower depths (≈30 m) in the Southern Caribbean due to upwelling-induced shoaling of isopycnals and slightly deeper (> 60 m) toward the north. Maximum mixed layer depths are typically reached in February, at the end of the cooling season (Montoya-Sánchez et al., 2018).

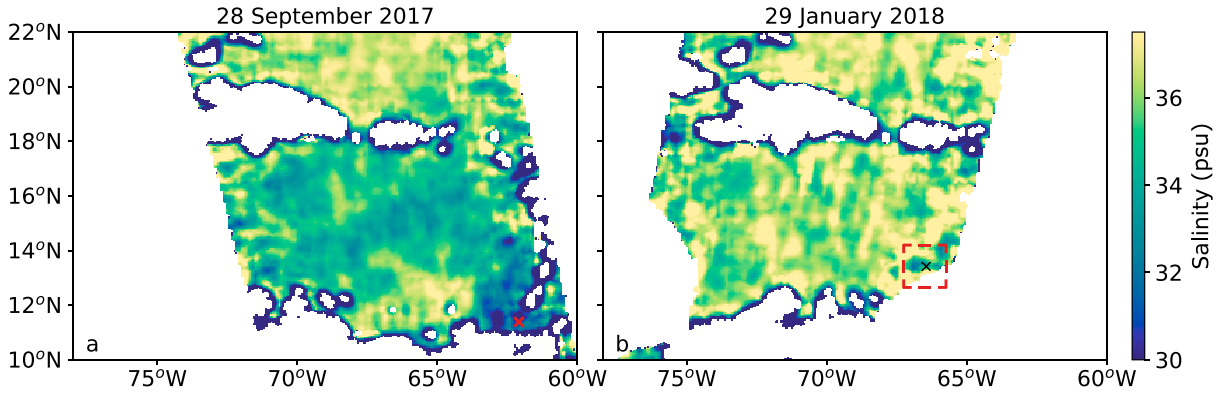

Figure 4. Sea surface salinity from the "Soil Moisture and Ocean Salinity" satellite on (a) 28 September 2017 and (b) 29 January 2018. The approximate formation region of the anticyclone is indicated with the red cross. The location of the anticyclone on 29 January 2018 was obtained from satellite altimetry with the py-eddy tracker and is indicated with the dashed square.

Our survey coincided with this cooling season. During the survey, winds measured and recorded by the underway logging system were consistently from the northeast with speeds of 10.0±1.7 m/s. The mixed layer at the CTD stations was confined by the halocline that separated the relatively fresh Caribbean surface waters from the saline Subtropical Underwater (STUW; see Appendix A). The mixed layers depth was between 40 and 80 dbar, with the deeper mixed layers located in the center of the anticyclone and on the northern side of the section (Figure 5a).

The mixed layer itself was depleted of nutrients, with PO_4 and NO_3 + NO_2 concentrations below 0.1 µmol/L, silicate concentration around 2 µmol/L, and low values for near-surface chlorophyll concentration (Figure A1). Below the mixed layer, concentrations increased sharply (Figure 5a). This sharp increase, which was still in the photic zone, coincided with a maximum in nutrients. At the core of the anticyclone, the deep chlorophyll maximum was found inside the barrier layer (outlined by the red and orange lines in Figure 5a), while it was located below the barrier layer outside the anticyclone.

In general, the Caribbean Sea is considered as an oligotrophic region, where the main region of productivity is found along the southern boundary (Muller-Karger et al., 1989; Muller-Karger & Castro, 1994), which is sustained by upwelling along the Venezuelan coast (Rueda-Roa & Muller-Karger, 2013). Farther north, increases in plankton are attributed to the more nutrient-rich inflow from the Amazon and Orinoco rivers (Hu et al., 2004; Muller-Karger et al., 1989).

The spatial gradient, seen in the chlorophyll data from the merged satellite product (Figure 5b), highlights lower concentrations of chlorophyll north of the position of the anticyclone, which is similar as observed during the survey (Figure 5a). These weak spatial changes at the surface were in strong contrast to the much

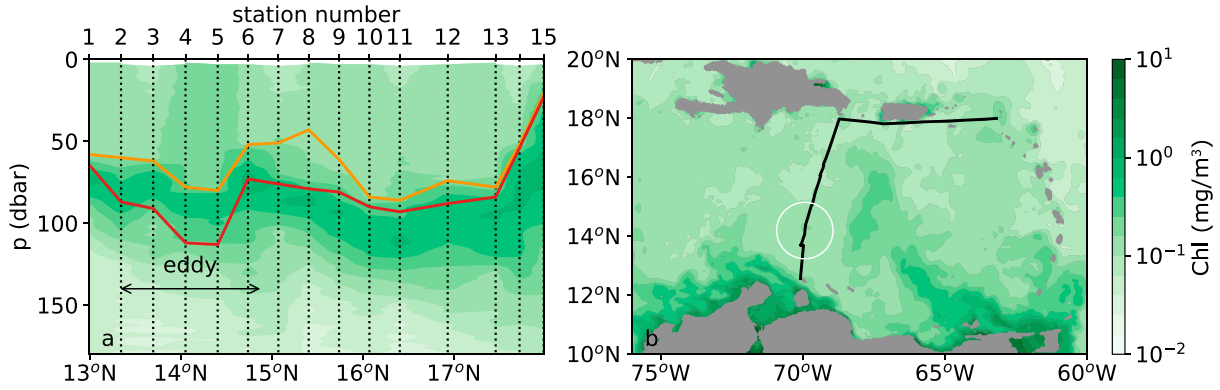

Figure 5. (a) Chlorophyll a fluorescence concentrations (mg/m^3) along the hydrographic section. The thermocline and halocline, indicated with the red and orange lines respectively, were computed following Mignot et al. (2012). (b) Surface chlorophyll concentrations from merged satellite products on 5 February 2018 obtained from E.U. Copernicus Marine Service Information. The cruise track is shown by the black line, and the location of the eddy is indicated by the white circle. Note the logarithmic color scale.

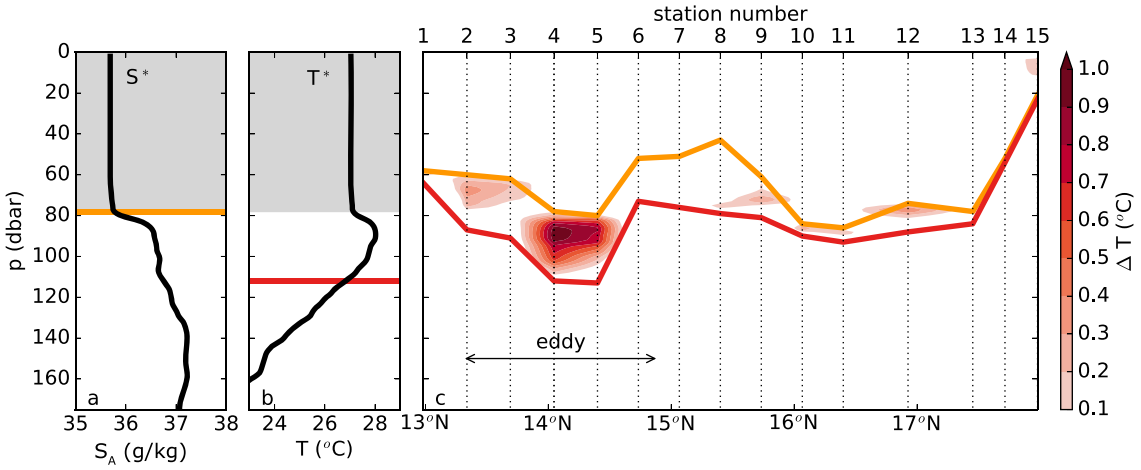

Figure 6. (a) Absolute salinity profile of the upper 180 dbar of the water column at station 4. The orange solid line shows the depth of the halocline at that location. The gray shaded area indicates the depth over which the mixed layer salinity (S^*) is determined. (b) Conservative temperature profile at station 4. The red solid line shows the depth of the thermocline, which was defined as the depth where the temperature decreased with 0.2 °C compared to the temperature of the mixed layer. The gray shaded area indicates the depth over which the mixed layer temperature (T^*) is determined. (c) Magnitude of the temperature inversion, defined as the temperature of the barrier layer minus the temperature of the mixed layer along the hydrographic section. The depth of the halocline and thermocline are indicated by the orange and red lines, respectively.

higher subsurface chlorophyll signal (Figure 5a). Higher surface concentrations were found south of the anticyclone, where strong trade winds forced coastal upwelling (Figure 5b).

At the core of the anticyclone, the observed surface chlorophyll concentration was enhanced (doubled in fact) compared to surrounding surface waters, although it was still quite low (Figure 5). Mesoscale eddies are known to alter the chlorophyll concentrations in various ways. The dominant mechanism is the horizontal advection of phytoplankton in the periphery of eddies (Chelton et al., 2011; Gaube et al., 2014). Chlorophyll anomalies can also be trapped in the core of the eddies (Early et al., 2011), of which the properties are altered by eddy-induced upwelling or downwelling (Gaube et al., 2013). In general, cyclones are considered more productive than anticyclones (Falkowski et al., 1991), but recently Dufois et al. (2016) showed that during winter anticyclones can be more productive than cyclones due to winter mixing in some parts of the Caribbean.

The elevated surface chlorophyll concentration inside the anticyclone implies that the anticyclone was more productive than its surroundings (Figure 5a). As we did not observe elevated levels of $NO_3 + NO_2$ concentrations in the core of the anticyclone (Figure A1f), it is unlikely that the observed enhancement is due to increased winter mixing. However, we found that these higher values coincide with slightly elevated silicate concentrations (Figure A1e), which we associated with the advection of the Orinoco River plume. Eastward of the anticyclone, surface chlorophyll values were higher compared to those in the anticyclone (Figure 5a). This offshore local maximum in surface chlorophyll east of the surveyed anticyclone was due to the offshore advection of nutrient-rich filaments of upwelled waters (Figure 5b). At that location, a cyclone and anticyclone were present (Figure 2). Apparently, these eddies (67°W, 14°N) trapped positive chlorophyll anomalies and advected these to the north.

3.3. Barrier Layer and Temperature Inversion

In the previous section, it was shown that the low salinity in the core of the anticyclone and the elevated productivity suggests that the anticyclone entrained waters from the Orinoco River plume. In combination with the larger mixed layer depth inside the anticyclone, the anticyclone became more susceptible for the formation of a thick barrier layer. Previous studies showed indeed that the surface waters in the Caribbean Sea are susceptible to the formation of barrier layers (Mignot et al., 2007; Rudzin et al., 2017). A barrier layer, defined as the layer between the top of the halocline and the top of the thermocline (Pailler et al., 1999), forms as a result of specific thermal and haline forcing (de Boyer Montégut et al., 2004). In general, heat is trapped in the barrier layer, which is released once the barrier layer gets eroded by intense atmospheric forcing (de Boyer Montégut et al., 2004). This heat release affects the heat transfer between the ocean and atmosphere, which has a potential important climatic impact (de Boyer Montégut et al., 2004). For example,

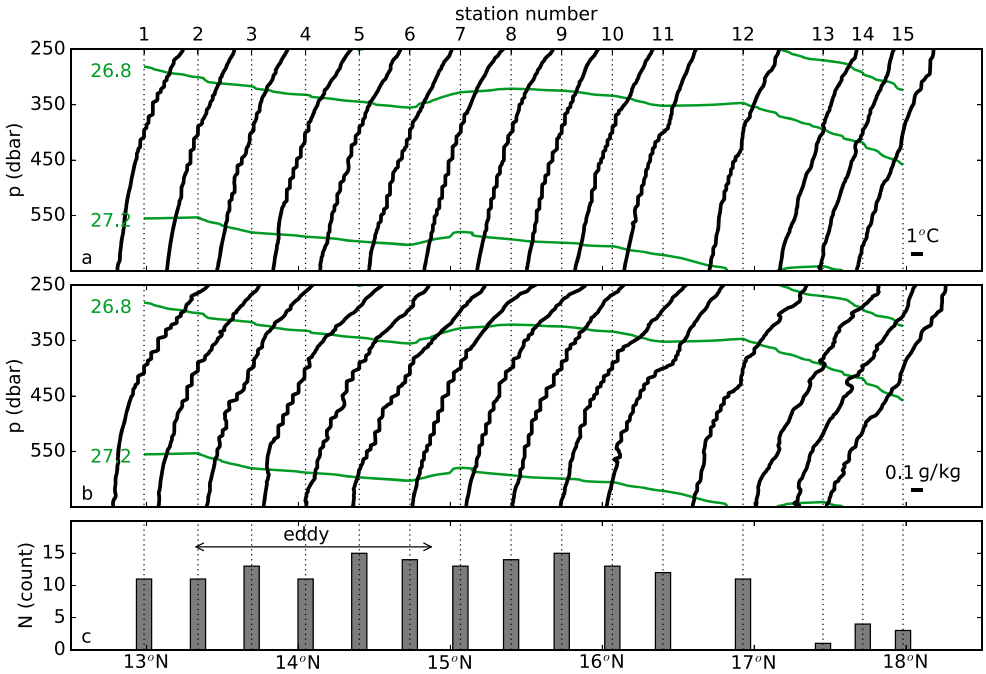

Figure 7. (a) Conservative temperature (°C) profiles and (b) absolute salinity (g/kg) profiles obtained with the CTD, between 250 and 650 dbar. σ contours are indicated. Each profile is projected upon the latitude of the station, indicated with the dashed black lines. The green lines show the density contours along the track. (c) The number of staircases that were found in each profile.

in the Caribbean Sea, this release of heat might enhance the growth of tropical cyclones (Balaguru et al., 2012).

The barrier layer thickness (BLT) is used as a proxy for the effects and strengths of the barrier layer (McPhaden & Foltz, 2013). During the hydrographic survey, a barrier layer was present in the southern part of the basin (Figure 6a). The thickest layers were observed within the core and at the periphery of the anticyclone (BLT = 35 ± 1 dbar). This is in line with observations of Rudzin et al. (2017), who found thicker barrier layers inside than outside their surveyed anticyclone.

In general, a strong halocline allows for the formation of temperature inversions inside barrier layers (Mignot et al., 2012). These temperature inversions have a strong seasonal cycle. The barrier layer warms due to solar radiation in summer (Masson & Delecluse, 2001). This heat is trapped in fall, when the mixed layer becomes less saline due to the river outflow (Mignot et al., 2007). During winter months, the mixed layer is cooled by the atmosphere, which leads to convective mixing (Montoya-Sánchez et al., 2018). This mixing tends to erode the top of the barrier layer and is limited by a strong halocline, allowing summer temperatures to be maintained in the barrier layer and creating a temperature inversion (Mignot et al., 2012).

During the survey, several temperature inversions were observed, which shows that the halocline was sufficiently strong to maintain a stable density stratification (Figure 6c). The strongest temperature inversion (+0.96 °C) was found in the thickest (≈35 dbar) and deepest (≈90 dbar) barrier layer. This is in line with Girishkumar et al. (2013) who showed that the magnitude of the temperature inversion correlates with the thickness of the barrier layer. The strongest temperature inversion was located at the core of the anticyclone, where low salinity anomalies in the mixed layer strengthened the salinity stratification. Furthermore, the barrier layer was located deeper in the water column due to the low density of the anticyclones. Both the salinity stratification and the deeper placement of the barrier layer are favorable conditions for the formation of temperature inversions (Girishkumar et al., 2013; Mignot et al., 2007).

3.4. Thermohaline Staircases

Below the mixed layer and barrier layer, a layer of strong vertical shear separated the surface-intensified flow from the weak flow below (Figures 3b and 3c). At the depth of these weak velocities, the temperature and salinity profiles obtained with the CTD clearly displayed thermohaline staircases (Figures 7a and 7b).

Similar staircase structures have been found before in this region (e.g., Lambert Jr & Sturges, 1977; Morell et al., 2006). They are formed by double diffusive mixing (salt fingers) between a warm and saline layer and a colder and fresher layer below. Double diffusive mixing occurs when the amount of turbulent mixing is low and the water mass has a low density ratio (R_ρ, Merryfield, 2000), defined as follows:

$$R_\rho = \frac{\alpha T_z}{\beta S_z}, \tag{1}$$

where T_z and S_z are the vertical gradients of potential temperature and absolute salinity, respectively. Here, α is the thermal expansion coefficient and β the haline contraction coefficient. If the density ratio is lower than 4, staircases may be observed in the ocean (Merryfield, 2000).

During the survey, staircases were present between 250 and 600 dbar in the density range of 26.6–27.2 kg/m^3 with a density ratio of $R_\rho = 1.7 \pm 0.2$ at $\sigma_0 = 27$ kg/m^3. Due to the meridional slope of the isopycnals, the staircases are found slightly higher in the water column in the south (Figure 7). Below the anticyclone, staircases were observed slightly deeper in the water column due to the eddy-induced isopycnal displacement. The staircases consisted of homogeneous layers with a thickness of 2–31 dbar. Most staircases were found within Tropical Atlantic Central Water (TACW; see Appendix A), where the temperature and salinity both decreased with depth, from the warm and saline STUW above toward the cold and less saline Antarctic Intermediate Water (AAIW) underneath. Staircase structures were weaker outside the TACW layer (Figure 7c), where the deep salinity minimum was slightly higher (Figure A1b).

The four Argo floats that were deployed have a parking depth of 500 dbar, at the depth of the staircase structures. As a result, the floats were advected with the staircases. Their profiles revealed that the staircases were persistent and that most staircases remained coherent structures for several weeks to several months. From deployment until September 2018, staircases were present at $\sigma_0 = 26.6$–27.2 kg/m^3. Within this layer, the average value of the density ratio was $R_\rho = 2.5 \pm 1.3$ at $\sigma_0 = 27.0$ kg/m^3.

4. Ecological Implication

The ecological impact of the surveyed anticyclone on the higher trophic levels was studied with a survey of the pelagic megafauna. The Caribbean Sea is known to be a global-scale hot spot for marine biodiversity (Roberts et al., 2002), but the marine biodiversity in the offshore and deep parts of the basin is undersampled (Miloslavich et al., 2010). In general, the coastal regions have a higher primary production (Andrade & Barton, 2005) and are more biodiverse than the oligotrophic offshore waters (Miloslavich et al., 2010). However, the dispersal of nutrient-rich upwelled waters and the advection of the river plumes by mesoscale anticyclones locally increase the productivity offshore.

In general, fish are known to be concentrated at fronts (Paramo et al., 2003; Wells et al., 2017), and the fronts of anticyclones are associated with upwelling (Bakun, 2006; Gaube et al., 2013; Seki et al., 2001). We observed a relatively high number of flying fish in coastal areas (Figure 8a), and a peak of flying fish was observed at 15°N (Figure 8a) that coincided with the northern front of the anticyclone (Figure 8c). Note that this front was observed with the thermosalinograph short after station 7, while the peak of flying fish was observed before station 7. Shortly after station 7, the sea surface salinity increased with approximately 0.2 g/kg, and sea surface temperature decreased with 0.3 °C from south to north. At the northern front, the depth of the mixed layer was slightly shallower (40 dbar), which might be related to frontal upwelling (Figure 5a). At the southern front of the anticyclone, we did not observe a similar peak of flying fish. The southern front of the anticyclone coincided with a strong coastal jet, and the depth of the mixed layer was slightly deeper (60 dbar). Also, small positive anomalies of $NO_3 + NO_2$ at both fronts suggest frontal upwelling (Figure A1f). Note that we do not have observations of fauna near the center of the eddy as these parts were surveyed during the night.

Along the 542 km that could be surveyed during daylight hours, we recorded in total 15 bird species, of which Brown Booby was the most abundant ($n = 276$; 62% of all birds recorded). It was seen throughout the whole survey area, but numbers were low during the northbound transects from Aruba to Hispaniola, that is, in the region of the eddy studied. We found very low bird densities in the central Caribbean and along the northern front of the anticyclone (Figure 8b), while potential prey (flying fish) seemed abundantly present (Figure 8a). That seabirds were largely absent from the central Caribbean may be explained by the generally low numbers of birds remaining in the Caribbean, due to loss of breeding habitat during the last

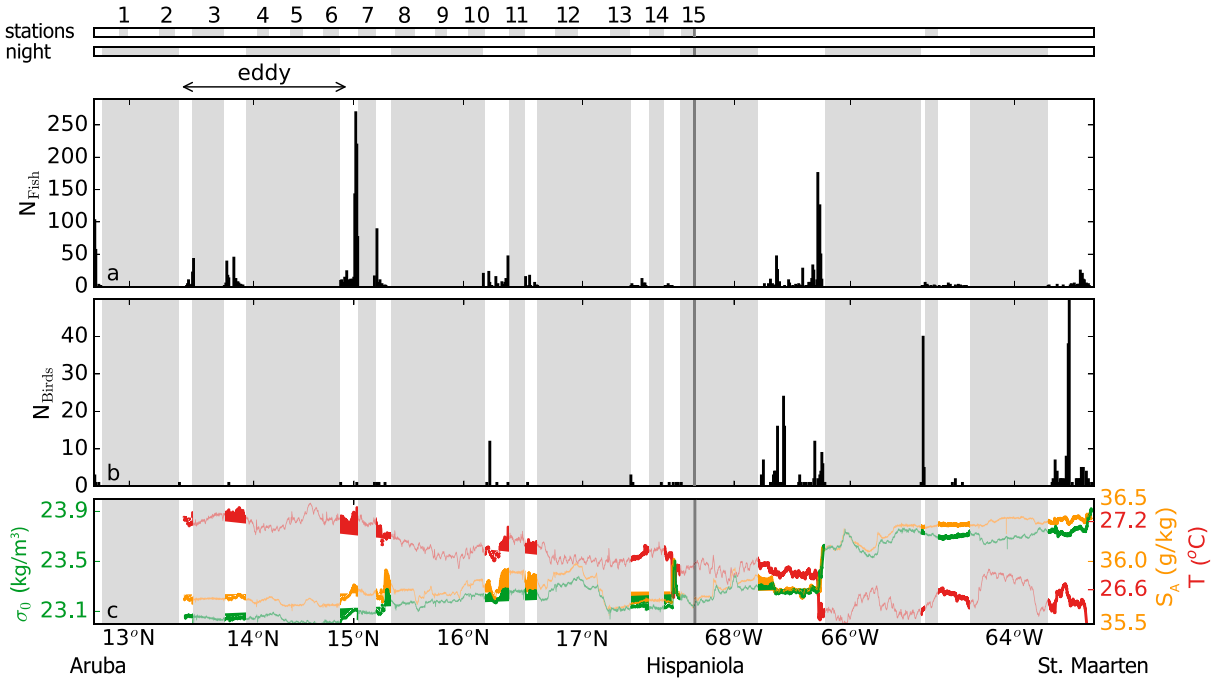

Figure 8. (a) Number of flying fish (N_{Fish}) observed along the track per 10-min count. (b) Number of birds (N_{Birds}) observed per 10-min count. (c) Surface temperature (T) , salinity (S_A), and density anomaly (σ_0) as observed with the shipboard thermosalinograph. The shaded gray regions indicate locations without observations during stations (top bar) and during nights (second bar). These periods without observations are also indicated by the shaded gray in panels a–c. The dark gray vertical solid line distinguishes the first part of the track (northward; hydrographic survey) from the second part (eastward en route to St. Maarten).

century (Lowrie et al., 2012; Van Halewijn & Norton, 1984). The remaining birds might not need to venture far offshore from their breeding colonies around the Caribbean Sea, since there is less competition today for prey closer to the breeding colonies, as seabirds have been depleted (Ashmole, 1963). In addition, the availability of prey far offshore might be unpredictable, so that other parts of the Caribbean might offer more predictable feeding opportunities, such as the coastal upwelling zones in the south of the basin. Far offshore, seabirds may have to rely on other predators that drive fish to the surface, such as large fish or cetaceans. Very few of these were seen during the survey.

5. Summary, Discussion, and Conclusions

We conducted a hydrographic and biological survey of a Caribbean anticyclone to gain insight into its origin, vertical structure, and ecological impact. The 180-km-wide anticyclone was surface intensified with the highest velocities located in the upper 150 m and along the southern perimeter of the anticyclone. Below 150 m, weaker velocities were observed, which might be caused by the passage of the shallow anticyclone above.

The anticyclone originated near Grenada Passage, which is similar to the anticyclone surveyed by Rudzin et al. (2017). Based on the low salinity and elevated silicate concentrations in the core of the anticyclone, we suggest that the anticyclone entrained surface waters originating from the Orinoco River. This is another source of salinity anomalies than suggested by Rudzin et al. (2017), who suspected that these anomalies originated from an NBC Ring. Ffield (2005) showed that the salinity of NBC Rings depends on the position of the Amazon River plume. The salinity anomalies found in this study as well as in the study of Rudzin et al. (2017) therefore highlight the importance of the Amazon and Orinoco River plumes on the formation and properties of Caribbean anticyclones.

The elevated silicate levels in the anticyclone coincided with an elevated chlorophyll concentration. This surface chlorophyll concentration in the center of the anticyclone was much lower than that in the nutrient-rich upwelling regions and lower than that at the deep chlorophyll maximum. This is in agreement with previous observations that the offshore regions in the Caribbean Sea are oligotrophic (Muller-Karger et al., 1989;

Muller-Karger & Castro, 1994). However, the small surface increase in chlorophyll concentration compared to the surroundings was significant and highlights that Caribbean anticyclones can be productive and thus can transport isolated ecosystems from the east to the western part of the basin.

The deep chlorophyll maximum was located below the mixed layer inside the barrier layer. The thickest barrier layers, which also contained a strong temperature inversion, were located in the core of the anticyclone. Based on Argo float profiles, de Boyer Montégut et al. (2007) found that maximum temperature inversions (0.6 °C in the Caribbean) occur in November and December. Although our survey took place in February, we observed much stronger temperature inversions (up to 0.98 °C) than found by de Boyer Montégut et al. (2007). Because temperature inversions form in winter as the mixed layer cools, we suggest that the expected magnitude of temperature inversions can be larger in late winter (February) than in early winter (November/December) if the barrier layer is located deep enough. This implies that previous estimates might have underestimated the magnitude of temperature inversions and that the heat trapped in the barrier layer is higher than expected. This could have important consequences, as this heat can be released during intense atmospheric forcing (de Boyer Montégut et al., 2007) and might be an additional energy source for developing hurricanes in this region.

Below the barrier layer, weak velocities due to isopycnal displacement were found. Because the sea level signature of the anticyclone and the tracks of the Argo floats that were deployed in the core of the anticyclone did not follow similar paths, it is plausible that waters at 500 dbar were not advected with the anticyclone. Therefore, we approximated the depth of the anticyclone to be 150 m, at the lower bound where we observed the highest velocities and where the shear decreases to the background value. This is shallower than the two estimates from previous observations of Caribbean anticyclones, where Rudzin et al. (2017) and Silander (2005) estimated depths of 500 and 1,400 m, respectively. Although these differences seem large, the anticyclone observed by Silander (2005) had a similar surface-intensified flow structure. Also, the velocities of the anticyclone observed by Rudzin et al. (2017) have a surface-intensified pattern, which reveals the possibility that all three anticyclones were shallow and the weak isopycnal displacement at depth was induced by the anticyclone above. Therefore, we think that most Caribbean anticyclones transport only water in the upper layer, while the passage of the shallow anticyclone induces a weak depression of the isopycnals at larger depths.

Below the anticyclone, we observed thermohaline staircases in the TACW layer. Based on the tracks of the deployed Argo floats, we showed that the thermohaline staircases were not advected with the anticyclone. This is in line with the observation that the anticyclone was shallow and that the weak isopycnal displacements in this layer were induced by the presence of the anticyclone above. This might also explain why we did not find a clear difference in staircase presence between the core and the periphery of the anticyclone, in contrast to previous studies (Bebieva & Timmermans, 2016; Morell et al., 2006; Silander, 2005).

The presence of the anticyclone altered the local ecology slightly, as shown by elevated chlorophyll concentrations in the core. The anticyclone contained a source of nutrients (Si), and a peak of flying fish was observed at its northern front. However, it seemed to be too far offshore to attract birds. The low densities of birds that were observed are a matter of concern and could be related to the loss of breeding habitat offshore (Lowrie et al., 2012; Van Halewijn & Norton, 1984).

Appendix A: Distribution of Water Masses

The Caribbean Sea is highly stratified and contains six water masses with distinctive properties (Hernández-Guerra & Joyce, 2000; Morrison & Nowlin, 1982). The surface waters of much of the Caribbean Sea consist of Caribbean Surface Water (CSW) that is characterized by salinities below 36 psu (Morrison & Nowlin, 1982). In general, marine nutrients are limited in CSW (Hansell & Follows, 2008), except during periods of maximum river discharge of the Amazon and Orinoco Rivers when CSW is mixed with the silicate-rich river outflow (Corredor & Morell, 2001; Froelich et al., 1978). This mixing results in the dispersal of patches of low salinity anomalies that can be found up to several hundreds of kilometers from the river outflow and can be identified by an elevated silicate concentrations (Corredor & Morell, 2001; Morell & Corredor, 2001). In our observations, CSW had an average temperature and salinity of $T = 26.9 \pm 0.2$ °C and $S_A = 35.8 \pm 0.1$ g/kg, respectively (Figures A1a and A1b).

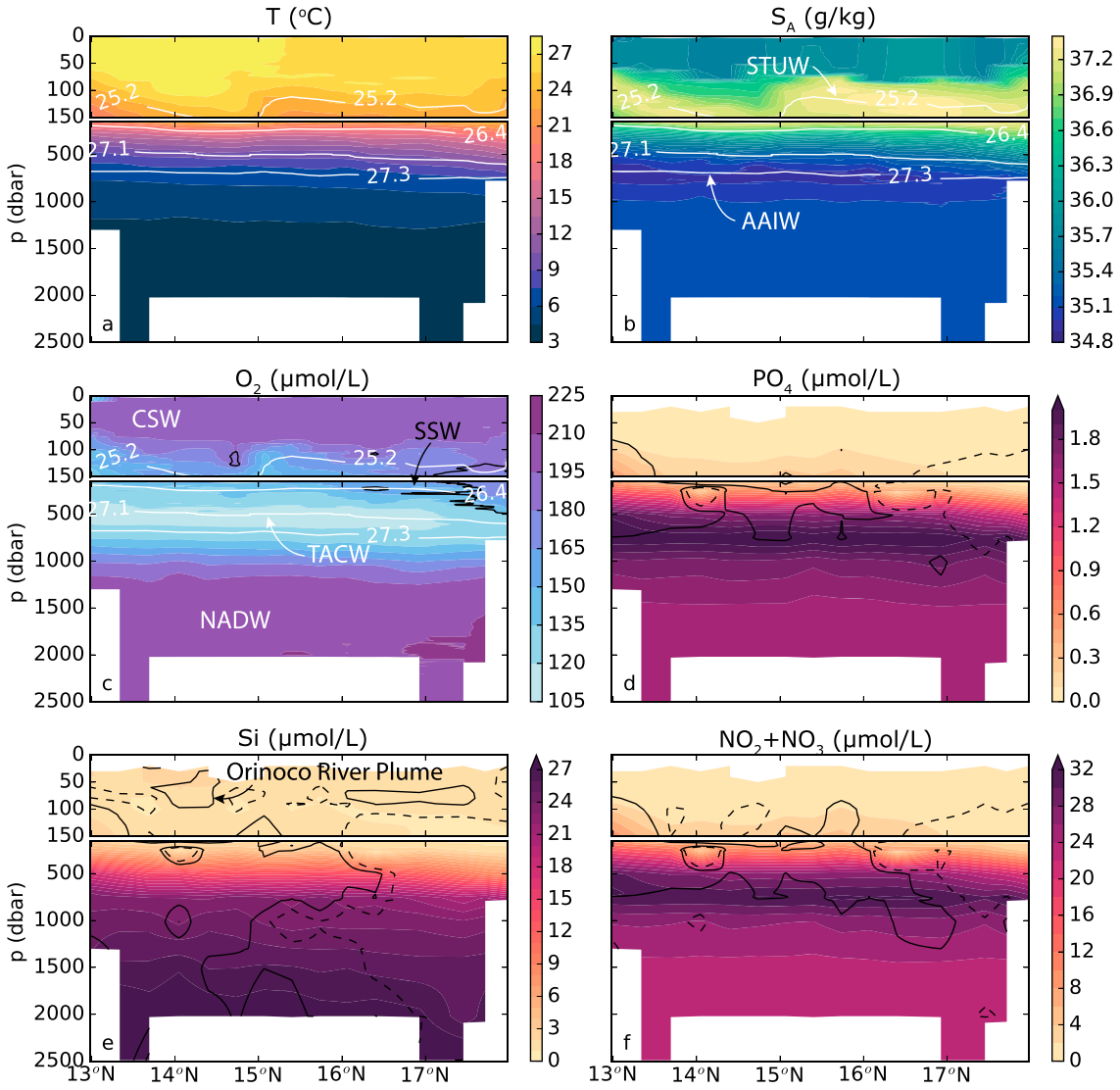

Figure A1. Section of conservative temperature (T), absolute salinity (S_A), oxygen (O_2), phosphate (PO_4), silicate (Si), and combined nitrate and nitrite (NO_3 + NO_2) along the cruise track. Indicated water masses are AAIW = Antarctic Intermediate Water, CSW = Caribbean Surface Water, NADW = North Atlantic Deep Water, SSW = Sargasso Sea Water, STUW = Subtropical Underwater, TACW = Tropical Atlantic Central Water. The white contour lines indicate the isopycnals in the core of a water mass. The black contour lines show positive (solid) and negative (dashed) anomalies from the depth-averaged mean for O_2 (contour drawn at 15 µmol/L), PO_4 (contour drawn at −0.05 and 0.05 µmol/L), Si (contour drawn at −0.2 and 0.2 µmol/L), and NO_3 + NO_2 (contour drawn at −0.5 and 0.5 µmol/L).

A strong halocline separates CSW from the saline STUW (Morrison & Nowlin, 1982; O'Connor et al., 2005). STUW is characterized by salinities (S_P) exceeding 37 psu. It originates from regions with high evaporation in the central tropical Atlantic Ocean and enters the Caribbean Sea in the northeast (Figure A2; Morrison & Nowlin, 1982; Montes et al., 2016; Wüst, 1964). The depth at which STUW is found decreases toward the Venezuelan coast, where it is upwelled and transports nutrients toward the surface (Montes et al., 2016; Rueda-Roa & Muller-Karger, 2013). In line with Morrison and Nowlin (1982) and Hernández-Guerra and Joyce (2000), we found the highest salinities in the northern part of the basin where the STUW is less diluted (Figure A1b). In addition, we found that the core of the STUW followed the σ_0 = 25.2 kg/m^3 isopycnal and varied in depth over the hydrographic section between 100 and 150 dbar.

Small patches of Sargasso Sea Water (SSW) enter the Caribbean Sea through the Anegada-Jungfern Passage at approximately 300 dbar (Figure A2; Morrison & Nowlin, 1982). SSW can be identified by (slightly) elevated levels of oxygen concentrations. The signal weakens along its path toward the southern part of the basin, because of the aging of this water mass (Kinard et al., 1974). We identified patches of SSW by oxygen

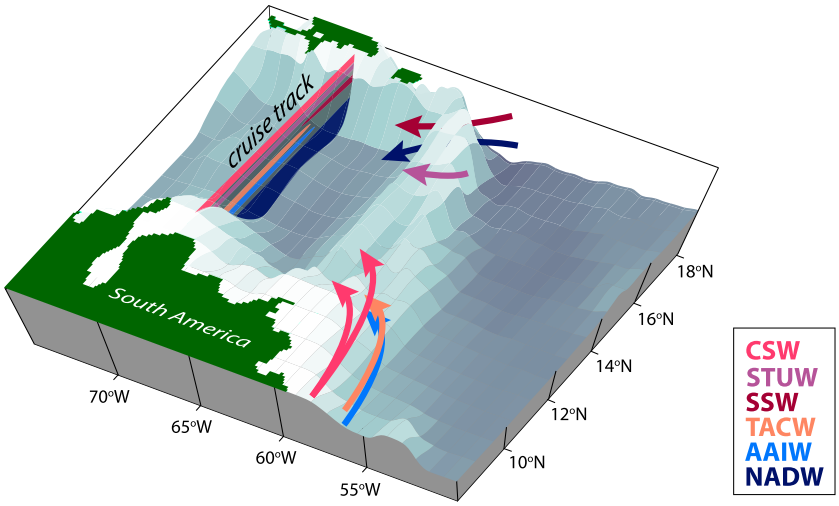

Figure A2. A 3-D schematic of how water masses enter the Caribbean Sea. The position of the water masses during the survey are indicated by color along the cruise track. Indicated water masses are AAIW = Antarctic Intermediate Water, CSW = Caribbean Surface Water, NADW = North Atlantic Deep Water, SSW = Sargasso Sea Water, STUW = Subtropical Underwater, TACW = Tropical Atlantic Central Water.

concentrations that were approximately 10 μmol/L higher than the surrounding values (Figure A1c). These patches followed the $\sigma_0 = 26.4$ kg/m^3 isopycnal, which sloped upward toward 150 dbar near the Venezuelan coast.

Below the patches of SSW, an oxygen minimum indicated the presence of TACW (Figure A1c). TACW originates in the tropical Atlantic Ocean and enters the Caribbean Sea through the southeastern passages (Figure A2; Metcalf, 1976; Morrison & Nowlin, 1982). Although the origin of this oxygen depletion in this layer remains unclear, the mean current pattern suggest that TACW originates near Angola (Portela et al., 2018). We found that the core of TACW ($O_2 < 120$ μmol/L) was located at the $\sigma_0 = 27.1$ kg/m^3 isopycnal at approximately 500 dbar and had a temperature of 9.3 ± 1.2 °C and a salinity of 35.2 ± 0.2 g/kg.

AAIW enters the Caribbean Sea through the same passages as TACW but at greater depths (Figure A2). AAIW can be identified by a salinity minimum and a phosphate and nitrate maximum (Morrison & Nowlin, 1982). This water mass originates from the Southern Ocean and propagates northward into the Atlantic Ocean at depths ranging between 500 and 1,000 m (Tsuchiya, 1989). Figures A1b, A1d, and A1f show that the core of AAIW was located at approximately 700 dbar. The core had an average salinity of 35.0 ± 0.02 g/kg and a temperature of 6.6 ± 0.4 °C.

The deep waters of the Caribbean Sea consist of strongly diluted North Atlantic Deep Water (Joyce et al., 1999). This water mass originates from the North Atlantic Ocean and enters the Caribbean Sea through Anegada-Jungfern Passage in the northeast of the Caribbean Sea (Figure A2; Morrison & Nowlin, 1982). Because this deep passage is shallower than the depth of the Caribbean Sea, the deeper parts of the Caribbean Sea are not in contact with the rest of the Atlantic Ocean. In line with previous observations (Joyce et al., 1999; Morrison & Nowlin, 1982), we found that North Atlantic Deep Water was vertically homogeneous below 1,800 dbar (Figure A1) and had an average temperature of 3.91 ± 0.03 °C and an average salinity of 35.2 ± 10^{-3} g/kg.

Acronyms

AAIW Antarctic Intermediate Water
CMEMS Copernicus Marine Environment Monitoring Service
CSW Caribbean Surface Water
CTD conductivity, temperature, depth
NBC North Brazil Current
SLA sea level anomaly
SSW Sargasso Sea Water

STUW Subtropical Underwater
TACW Tropical Atlantic Central Water
VMADCP vessel-mounted acoustic Doppler current profiler

Acknowledgments
For this paper we acknowledge the funding of the Netherlands Organisation for Scientific Research NWO and Royal Netherlands Institute for Sea Research NIOZ in organizing the Netherlands Initiative Changing Oceans NICO expedition in 2018. The work on marine mammals and seabirds was partly funded through the WUR/EKZ Project BO43 Yarari. The work of Carine van der Boog is financed by a Delft Technology Fellowship awarded to Caroline Katsman by Delft University of Technology. Financial support of Kirstin Schulz was provided by the STW project "Sediment for the salt marches: Physical and ecological aspects of a mud motor" (Grant 13888). We would like to thank the crew of the RV *Pelagia* and TU Delft Master students Ophélie Meuriot and Tolga Cömert for their help on board and with processing the data. We thank Rob Buiter for his contribution to the megafauna survey. We also appreciated the discussions before and after the cruise with the SCENES group (http://www.staff.science.uu.nl/~dijks101/SCENES/), in particular with Adam Candy. This study has been conducted using E.U. Copernicus Marine Service Information (http://marine.copernicus.eu). The Argo data is freely available at the Coriolis Argo Global Data Assembly Centre (ftp://ftp.ifremer.fr/ifremer/argo/, http://doi.org/10.17882/42182). The survey data are available online (https://doi.org/10.17882/59178).

References

Alvera-Azcárate, A., Barth, A., & Weisberg, R. H. (2009). The surface circulation of the Caribbean Sea and the Gulf of Mexico as inferred from satellite altimetry. *Journal of Physical Oceanography*, *39*(3), 640–657. https://doi.org/10.1175/2008JPO3765.1

Andrade, C. A., & Barton, E. D. (2000). Eddy development and motion in the Caribbean Sea. *Journal of Geophysical Research*, *105*(C11), 26,191–26,201. https://doi.org/10.1029/2000JC000300

Andrade, C. A., & Barton, E. D. (2005). The Guajira upwelling system. *Continental Shelf Research*, *25*(9), 1003–1022. https://doi.org/10.1016/j.csr.2004.12.012

Ashmole, N. P. (1963). The regulation of numbers of tropical oceanic birds. *Ibis*, *103*(3), 458–473.

Bakun, A. (2006). Fronts and eddies as key structures in the habitat of marine fish larvae: Opportunity, adaptive response and competitive advantage. *Scientia Marina*, *70*(S2), 105–122. https://doi.org/10.3989/scimar.2006.70s2105

Balaguru, K., Chang, P., Saravanan, R., & Jang, C. J. (2012). The barrier layer of the Atlantic warmpool: Formation mechanism and influence on the mean climate. *Tellus A: Dynamic Meteorology and Oceanography*, *64*(1), 18162. https://doi.org/10.3402/tellusa.v64i0.18162

Bebieva, Y., & Timmermans, M.-L. (2016). An examination of double-diffusive processes in a mesoscale eddy in the Arctic Ocean. *Journal of Geophysical Research: Oceans*, *121*, 457–475. https://doi.org/10.1002/2015JC011105

Bertrand, S., Gohin, F., & Garello, R. (2009). Regional objective analysis for merging MERIS, MODIS/aqua and SeaWiFS chlorophyll-a data from 1998 to 2008 on the European Atlantic Shelf at a resolution of 1.1 km, *Oceans 2009-Europe* (pp. 1–10). Bremen, Germany: IEEE.

Bidigare, R. R., Ondrusek, M. E., & Brooks, J. M. (1993). Influence of the Orinoco River outflow on distributions of algal pigments in the Caribbean Sea. *Journal of Geophysical Research*, *98*(C2), 2259–2269. https://doi.org/10.1029/92JC02762

Camphuysen, C. J., & Garthe, S. (2004). Recording foraging seabirds at sea: Standardised recording and coding of foraging behaviour and multi-species foraging associations. *Atlantic Seabirds*, *5*, 1–23.

Carton, J. A., & Chao, Y. (1999). Caribbean Sea eddies inferred from TOPEX/Poseidon altimetry and a 1/6 Atlantic Ocean model simulation. *Journal of Geophysical Research*, *104*(C4), 7743–7752. https://doi.org/10.1029/1998JC900081

Centurioni, L. R., & Niiler, P. P. (2003). On the surface currents of the Caribbean Sea. *Geophysical Research Letters*, *30*(6), 1279. https://doi.org/10.1029/2002GL016231

Chang, Y., & Oey, L. (2013). Coupled response of the trade wind, SST gradient, and SST in the Caribbean Sea, and the potential impact on Loop Current's interannual variability*. *Journal of Physical Oceanography*, *43*(7), 1325–1344. https://doi.org/10.1175/JPO-D-12-0183.1

Chelton, D. B., Gaube, P., Schlax, M. G., Early, J. J., & Samelson, R. M. (2011). The influence of nonlinear mesoscale eddies on near-surface oceanic chlorophyll. *Science*, *334*(6054), 328–332. https://doi.org/10.1126/science.1208897

Chérubin, L., & Richardson, P. (2007). Caribbean current variability and the influence of the Amazon and Orinoco freshwater plumes. *Deep Sea Research Part I: Oceanographic Research Papers*, *54*(9), 1451–1473. https://doi.org/10.1016/j.dsr.2007.04.021

Corredor, J. E., & Morell, J. M. (2001). Seasonal variation of physical and biogeochemical features in eastern Caribbean Surface Water. *Journal of Geophysical Research*, *106*(C3), 4517–4525. https://doi.org/10.1029/2000JC000291

Corredor, J., Morell, J., López, J., Armstrong, R., Dieppa, A., Cabanillas, C., et al. (2003). Remote continental forcing of phytoplankton biogeochemistry: Observations across the "Caribbean-Atlantic front". *Geophysical Research Letters*, *30*(20), 2057. https://doi.org/10.1029/2003GL018193

Corredor, J. E., Morell, J. M., Lopez, J. M., Capella, J. E., & Armstrong, R. A. (2004). Cyclonic eddy entrains Orinoco River Plume in eastern Caribbean. *Eos, Transactions American Geophysical Union*, *85*(20), 197–202. https://doi.org/10.1029/2004EO200001

de Boyer Montégut, C., Madec, G., Fischer, A. S., Lazar, A., & Iudicone, D. (2004). Mixed layer depth over the global ocean: An examination of profile data and a profile-based climatology. *Journal of Geophysical Research*, *109*, C12003. https://doi.org/10.1029/2004JC002378

de Boyer Montégut, C., Mignot, J., Lazar, A., & Cravatte, S. (2007). Control of salinity on the mixed layer depth in the world ocean: 1. General description. *Journal of Geophysical Research*, *112*, C06011. https://doi.org/10.1029/2006JC003953

de Jong, M. F. (2018). *Cruise 64PE431: A south to north hydrographic transect in the central Caribbean Sea in February 2018*: SEANOE. https://doi.org/10.17882/59178, https://www.seanoe.org/data/00480/59178/

Dufois, F., Hardman-Mountford, N. J., Greenwood, J., Richardson, A. J., Feng, M., & Matear, R. J. (2016). Anticyclonic eddies are more productive than cyclonic eddies in subtropical gyres because of winter mixing. *Science Advances*, *2*(5), e1600282. https://doi.org/10.1126/sciadv.1600282

Early, J. J., Samelson, R. M., & Chelton, D. B. (2011). The evolution and propagation of quasigeostrophic ocean eddies*. *Journal of Physical Oceanography*, *41*(8), 1535–1555. https://doi.org/10.1175/2011JPO4601.1

Egbert, G. D., & Erofeeva, S. Y. (2002). Efficient inverse modeling of barotropic ocean tides. *Journal of Atmospheric and Oceanic Technology*, *19*(2), 183–204.

Ezer, T., Thattai, D. V., Kjerfve, B., & Heyman, W. D. (2005). On the variability of the flow along the Meso-American Barrier Reef system: A numerical model study of the influence of the Caribbean current and eddies. *Ocean Dynamics*, *55*(5-6), 458–475. https://doi.org/10.1007/s10236-005-0033-2

Falkowski, P. G., Ziemann, D., Kolber, Z., & Bienfang, P. K. (1991). Role of eddy pumping in enhancing primary production in the ocean. *Nature*, *352*(6330), 55. https://doi.org/10.1038/352055a0

Ffield, A. (2005). North Brazil current rings viewed by TRMM Microwave Imager SST and the influence of the Amazon Plume. *Deep Sea Research Part I: Oceanographic Research Papers*, *52*(1), 137–160. https://doi.org/10.1016/j.dsr.2004.05.013

Froelich, P. N. Jr., Atwood, D. K., & Giese, G. S. (1978). Influence of Amazon River discharge on surface salinity and dissolved silicate concentration in the Caribbean Sea. *Deep Sea Research*, *25*(8), 735–744. https://doi.org/10.1016/0146-6291(78)90627-6

Gaube, P., Chelton, D. B., Samelson, R. M., Schlax, M. G., & O'Neill, L. W. (2015). Satellite observations of mesoscale eddy-induced Ekman pumping. *Journal of Physical Oceanography*, *45*(1), 104–132. https://doi.org/10.1175/JPO-D-14-0032.1

Gaube, P., Chelton, D. B., Strutton, P. G., & Behrenfeld, M. J. (2013). Satellite observations of chlorophyll, phytoplankton biomass, and Ekman pumping in nonlinear mesoscale eddies. *Journal of Geophysical Research: Oceans*, *118*, 6349–6370. https://doi.org/10.1002/2013JC009027

Gaube, P., McGillicuddy, D. J., Chelton, D. B., Behrenfeld, M. J., & Strutton, P. G. (2014). Regional variations in the influence of mesoscale eddies on near-surface chlorophyll. *Journal of Geophysical Research: Oceans*, *119*, 8195–8220. https://doi.org/10.1002/2014JC010111

Gilbes, F., & Armstrong, R. A. (2004). Phytoplankton dynamics in the eastern Caribbean Sea as detected with space remote sensing. *International Journal of Remote Sensing*, *25*(7-8), 1449–1453. https://doi.org/10.1080/01431160310001592427

Girishkumar, M. S., Ravichandran, M., & McPhaden, M. J. (2013). Temperature inversions and their influence on the mixed layer heat budget during the winters of 2006–2007 and 2007–2008 in the Bay of Bengal. *Journal of Geophysical Research: Oceans*, *118*, 2426–2437. https://doi.org/10.1002/jgrc.20192

Hansell, D. A., & Follows, M. J. (2008). Nitrogen in the Atlantic Ocean, *Nitrogen in the marine environment* (2nd ed., pp. 597–630). Burlington, MA: Academic Press. https://doi.org/10.1016/B978-0-12-372522-6.00013-X

Hernández-Guerra, A., & Joyce, T. M. (2000). Water masses and circulation in the surface layers of the Caribbean at 66°W. *Geophysical Research Letters*, *27*(21), 3497–3500. https://doi.org/10.1029/1999GL011230

Hu, C., Montgomery, E. T., Schmitt, R. W., & Muller-Karger, F. E. (2004). The dispersal of the Amazon and Orinoco River water in the tropical Atlantic and Caribbean Sea: Observation from space and S-PALACE floats. *Deep Sea Research Part II: Topical Studies in Oceanography*, *51*(10-11), 1151–1171. https://doi.org/10.1016/j.dsr2.2004.04.001

Jouanno, J., & Sheinbaum, J. (2013). Heat balance and eddies in the Caribbean upwelling system. *Journal of Physical Oceanography*, *43*(5), 1004–1014. https://doi.org/10.1175/JPO-D-12-0140.1

Jouanno, J., Sheinbaum, J., Barnier, B., & Molines, J.-M. (2009). The mesoscale variability in the Caribbean Sea. Part II: Energy sources. *Ocean Modelling*, *26*(3-4), 226–239. https://doi.org/10.1016/j.ocemod.2008.10.006

Jouanno, J., Sheinbaum, J., Barnier, B., Molines, J.-M., Debreu, L., & Lemarié, F. (2008). The mesoscale variability in the Caribbean Sea. Part I: Simulations and characteristics with an embedded model. *Ocean Modelling*, *23*(3-4), 82–101. https://doi.org/10.1016/j.ocemod.2008.04.002

Joyce, T. M., Pickart, R. S., & Millard, R. C. (1999). Long-term hydrographic changes at 52 and 66°W in the North Atlantic Subtropical Gyre and Caribbean. *Deep Sea Research Part II: Topical Studies in Oceanography*, *46*(1-2), 245–278. https://doi.org/10.1016/S0967-0645(98)00102-7

Kermabon, C., Lherminier, P., Le Bot, P., & Gaillard, F. (2018). Cascade v7.2: Logiciel de validation et de visualisation des mesures ADCP de coque.

Kinard, W. F., Atwood, D. K., & Giese, G. S. (1974). Dissolved oxygen as evidence for 18°C Sargasso Sea Water in the eastern Caribbean Sea. *Deep Sea Research and Oceanographic Abstracts*, *21*(1), 79–82. https://doi.org/10.1016/0011-7471(74)90021-7

Lambert Jr, R. B., & Sturges, W. (1977). A thermohaline staircase and vertical mixing in the thermocline. *Deep Sea Research*, *24*(3), 211–222. https://doi.org/10.1016/S0146-6291(77)80001-5

Lowrie, K., Lowrie, D., & Collier, N. (2012). *Seabird breeding atlas of the Lesser Antilles* (pp. 221). North Carolina: Environmental Protection in the Caribbean (EPIC).

Madec, G. (2015). *NEMO ocean engine*. Paris, France: Institut Pierre-Simon Laplace.

Mason, E., Pascual, A., & McWilliams, J. C. (2014). A new sea surface height based code for oceanic mesoscale eddy tracking. *Journal of Atmospheric and Oceanic Technology*, *31*(5), 1181–1188. https://doi.org/10.1175/JTECH-D-14-00019.1

Masson, S., & Delecluse, P. (2001). Influence of the Amazon River runoff on the tropical Atlantic. *Physics and Chemistry of the Earth, Part B: Hydrology, Oceans and Atmosphere*, *26*(2), 137–142. https://doi.org/10.1016/S1464-1909(00)00230-6

McPhaden, M. J., & Foltz, G. R. (2013). Intraseasonal variations in the surface layer heat balance of the central equatorial Indian Ocean: The importance of zonal advection and vertical mixing. *Geophysical Research Letters*, *40*, 2737–2741. https://doi.org/10.1002/grl.50536

Merryfield, W. J. (2000). Origin of thermohaline staircases. *Journal of Physical Oceanography*, *30*(5), 1046–1068. https://doi.org/10.1175/1520-0485(2000)030<1046:OOTS>2.0.CO;2

Metcalf, W. G. (1976). Caribbean-Atlantic water exchange through the Anegada-Jungfern passage. *Journal of Geophysical Research*, *81*(36), 6401–6409. https://doi.org/10.1029/JC081i036p06401

Mignot, J. C., de Boyer Montégut, C., Lazar, A., & Cravatte, S. (2007). Control of salinity on the mixed layer depth in the world ocean: 2. Tropical areas. *Journal of Geophysical Research*, *112*, C10010. https://doi.org/10.1029/2006JC003954

Mignot, J., Lazar, A., & Lacarra, M. (2012). On the formation of barrier layers and associated vertical temperature inversions: A focus on the northwestern tropical Atlantic. *Journal of Geophysical Research*, *117*, C02010. https://doi.org/10.1029/2011JC007435

Miloslavich, P., Díaz, J. M., Klein, E., Alvarado, J. J., Díaz, C., Gobin, J., et al. (2010). Marine biodiversity in the Caribbean: Regional estimates and distribution patterns. *PLoS ONE*, *5*(8), e11916. https://doi.org/10.1371/journal.pone.0011916

Molinari, R. L., Spillane, M., Brooks, I., Atwood, D., & Duckett, C. (1981). Surface currents in the Caribbean Sea as deduced from Lagrangian observations. *Journal of Geophysical Research*, *86*(C7), 6537–6542. https://doi.org/10.1029/JC086iC07p06537

Molleri, G. S., Novo, E. M. M., & Kampel, M. (2010). Space-time variability of the Amazon River plume based on satellite ocean color. *Continental Shelf Research*, *30*(3-4), 342–352. https://doi.org/10.1016/j.csr.2009.11.015

Montes, E., Muller-Karger, F. E., Cianca, A., Lomas, M. W., Lorenzoni, L., & Habtes, S. (2016). Decadal variability in the oxygen inventory of North Atlantic subtropical underwater captured by sustained, long-term oceanographic time series observations. *Global Biogeochemical Cycles*, *30*, 460–478. https://doi.org/10.1002/2015GB005183

Montoya-Sánchez, R., Devis-Morales, A., Bernal, G., & Poveda, G. (2018). Seasonal and interannual variability of the mixed layer heat budget in the Caribbean Sea. *Journal of Marine Systems*, *187*(May), 111–127. https://doi.org/10.1016/j.jmarsys.2018.07.003

Morell, J. M., & Corredor, J. E. (2001). Photomineralization of fluorescent dissolved organic matter in the Orinoco River plume: Estimation of ammonium release. *Journal of Geophysical Research*, *106*(C8), 16,807–16,813. https://doi.org/10.1029/1999JC000268

Morell, J. M., Corredor, J. E., & Merryfield, W. J. (2006). Thermohaline staircases in a Caribbean eddy and mechanisms for staircase formation. *Deep Sea Research Part II: Topical Studies in Oceanography*, *53*(1-2), 128–139. https://doi.org/10.1016/j.dsr2.2005.09.013

Morrison, J. M., & Nowlin, W. D. (1982). General distribution of water masses within the eastern Caribbean Sea during the winter of 1972 and fall of 1973. *Journal of Geophysical Research*, *87*(C6), 4207. https://doi.org/10.1029/JC087iC06p04207

Muller-Karger, F. E., & Castro, R. A. (1994). Mesoscale processes affecting phytoplankton abundance in the southern Caribbean Sea. *Continental Shelf Research*, *14*(2-3), 199–221. https://doi.org/10.1016/0278-4343(94)90013-2

Muller-Karger, F., McClain, C., Fisher, T., Esaias, W., & Varela, R. (1989). Pigment distribution in the Caribbean sea: Observations from space. *Progress in Oceanography*, *23*(1), 23–64. https://doi.org/10.1016/0079-6611(89)90024-4

Nystuen, J. A., & Andrade, C. A. (1993). Tracking mesoscale ocean features in the Caribbean Sea using Geosat altimetry. *Journal of Geophysical Research*, *98*(C5), 8389–8394. https://doi.org/10.1029/93JC00125

O'Connor, B. M., Fine, R. A., & Olson, D. B. (2005). A global comparison of subtropical underwater formation rates. *Deep Sea Research Part I: Oceanographic Research Papers*, *52*(9), 1569–1590. https://doi.org/10.1016/j.dsr.2005.01.011

Oey, L.-Y., Ezer, T., & Lee, H.-C. (2005). Loop Current, rings and related circulation in the Gulf of Mexico: A review of numerical models and future challenges. In L.-Y. Oey, T. Ezer, & H.-C. Lee (Eds.), *Circulation in the Gulf of Mexico: Observations and models* (pp. 31–56). Washington, DC: American Geophysical Union. https://doi.org/10.1029/161GM04

Oey, L., Lee, H., & Schmitz, W. Jr. (2003). Effects of winds and Caribbean eddies on the frequency of Loop Current eddy shedding: A numerical model study. *Journal of Geophysical Research*, *108*(C10), 3324. https://doi.org/10.1029/2002JC001698

Pailler, K., Bourlés, B., & Gouriou, Y. (1999). The barrier layer in the western tropical Atlantic Ocean. *Geophysical Research Letters*, *26*(14), 2069–2072. https://doi.org/10.1029/1999GL900492

Paramo, J., Quiñones, R. A., Ramirez, A., & Wiff, R. (2003). Relationship between abundance of small pelagic fishes and environmental factors in the Colombian Caribbean Sea: An analysis based on hydroacoustic information. *Aquatic Living Resources*, *16*(3), 239–245. https://doi.org/10.1016/S0990-7440(03)00043-3

Portela, E., Tenreiro, M., Pallás-Sanz, E., Meunier, T., Ruiz-Angulo, A., Sosa-Gutiérrez, R., & Cusí, S. (2018). Hydrography of the central and western Gulf of Mexico. *Journal of Geophysical Research: Oceans*, *123*, 5134–5149. https://doi.org/10.1029/2018JC013813

Richardson, P. (2005). Caribbean Current and eddies as observed by surface drifters. *Deep Sea Research Part II: Topical Studies in Oceanography*, *52*(3-4), 429–463. https://doi.org/10.1016/j.dsr2.2004.11.001

Roberts, C. M., McClean, C. J., Veron, J. E. N., Hawkins, J. P., Allen, G. R., McAllister, D. E., et al. (2002). Marine biodiversity hotspots and conservation priorities for tropical reefs. *Science*, *295*(5558), 1280–1284. https://doi.org/10.1126/science.1067728

Rudzin, J. E., Shay, L. K., Jaimes, B., & Brewster, J. K. (2017). Upper ocean observations in eastern Caribbean Sea reveal barrier layer within a warm core eddy. *Journal of Geophysical Research: Oceans*, *122*, 1057–1071. https://doi.org/10.1002/2016JC012339

Rueda-Roa, D. T., & Muller-Karger, F. E. (2013). The southern Caribbean upwelling system: Sea surface temperature, wind forcing and chlorophyll concentration patterns. *Deep Sea Research Part I: Oceanographic Research Papers*, *78*, 102–114. https://doi.org/10.1016/j.dsr.2013.04.008

Seki, M. P., Polovina, J. J., Brainard, R. E., Bidigare, R. R., Leonard, C. L., & Foley, D. G. (2001). Biological enhancement at cyclonic eddies tracked with GOES thermal imagery in Hawaiian waters. *Geophysical Research Letters*, *28*(8), 1583–1586. https://doi.org/10.1029/2000GL012439

Silander, M. F. (2005). *On the three-dimensional structure of Caribbean mesoscale eddies* (pp. 1–91). San Juan, Puerto Rico: University of Puerto Rico.

Simmons, H. L., & Nof, D. (2002). The squeezing of eddies through gaps. *Journal of Physical Oceanography*, *32*(1), 314–335. https://doi.org/10.1175/1520-0485(2002)032<0314:TSOETG>2.0.CO;2

Tasker, M. L., Jones, P. H., Dixon, T., & Blake, B. F. (1984). Counting seabirds at sea from ships: A review of methods employed and a suggestion for a standardized approach. *The Auk*, *101*(3), 567–577.

Taylor, M. A., & Alfaro, E. J. (2005). *Central America and the Caribbean, climate of* (pp. 183–189). Netherlands, Dordrecht: Springer. https://doi.org/10.1007/1-4020-3266-8_37

Tsuchiya, M. (1989). Circulation of the Antarctic Intermediate Water in the North Atlantic Ocean. *Journal of Marine Research*, *47*(4), 747–755. https://doi.org/10.1357/002224089785076136

Van Halewijn, R., & Norton, R. L. (1984). Status and conservation of seabirds of the Caribbean. In J. Croxall, P. Evans, & R. Schreiber (Eds.), *Status and conservation of the world's seabirds* (pp. 169–222). Cambridge, UK: International council on bird preservation technical publication 2.

Wells, R. J. D., Rooker, J. R., Quigg, A., & Wissel, B. (2017). Influence of mesoscale oceanographic features on pelagic food webs in the Gulf of Mexico. *Marine Biology*, *164*(4), 92. https://doi.org/10.1007/s00227-017-3122-0

Wüst, G. (1964). *Stratification and circulation in the Antillean-Caribbean basins*, vol. 1. Columbia: Columbia University Press.